

THE IMPORTANCE OF PHYSICAL MODELS FOR DERIVING DUST MASSES IN SUPERNOVA EJECTA I: RADIATIVELY HEATED DUST SURROUNDING THE CRAB'S PULSAR WIND NEBULA

TEA TEMIM^{1,2}, ELI DWEK¹

Submitted to The Astrophysical Journal, Feb 21, 2013

ABSTRACT

Recent far-infrared (IR) observations of supernova remnants (SNRs) have revealed significantly large amounts of newly-condensed dust in their ejecta, comparable to the total mass of available refractory elements. The dust masses derived from these observations assume that all the grains of a given species radiate at the same temperature, regardless of the dust heating mechanism or grain radius. In this paper, we derive the dust mass in the ejecta of the Crab Nebula, using a physical model for the heating and radiation from the dust. We adopt a power-law distribution of grain sizes and two different dust compositions, and calculate the heating rate of each dust grain by the radiation from the pulsar wind nebula (PWN). We find that the grains attain a continuous range of temperatures, depending on their size and composition. The best-fit model to the observed IR spectrum consist of amorphous carbon grains with a total mass of $0.027 \pm 0.003 M_{\odot}$. We find that the power-law size distribution of dust grains is characterized by a power-law index of 3.5 and a maximum grain size larger than $0.6 \mu\text{m}$. The grain sizes and composition are consistent with what is expected for dust grains formed in a Type IIP SN. Our derived dust mass is significantly less than the $0.11\text{--}0.24 M_{\odot}$ reported in previous studies of the Crab Nebula that are based on a simplified two-temperature models. These models also require a larger mass of refractory elements to be locked up in dust than was likely available in the ejecta. The results of this study shows that a physical model resulting in a realistic distribution of dust temperatures can significantly affect derived dust masses. Our study has therefore important implications for dust mass estimates in other SNRs and for the ultimate question of whether SNe are major sources of dust in the Galactic interstellar medium (ISM) and in external galaxies.

Subject headings: dust, extinction - infrared: ISM - ISM: individual objects (Crab Nebula) - ISM: supernova remnants - pulsars: individual (PSR B0531+21)

1. INTRODUCTION

In recent years, the far-infrared (IR) observations of supernova remnants (SNRs) with the *Herschel Space Observatory* have allowed us to finally tackle the longstanding question of whether supernovae (SNe) contribute a significant amount of dust to the interstellar medium (ISM). Theoretical dust condensation models predict that $0.1\text{--}0.7 M_{\odot}$ of dust should form in a SN explosion (Todini & Ferrara 2001; Cherchneff & Dwek 2010; Nozawa et al. 2010; Silvia et al. 2012), with $\sim 40\%$ surviving the reverse shock and being injected into the surrounding ISM (e.g., Dwek et al. 2008; Kozasa et al. 2009). Observations of dusty galaxies at high redshifts also imply that large quantities of dust are produced on short timescales, requiring $0.1\text{--}1.0 M_{\odot}$ of dust to be produced by an average SN explosion, depending on the dust lifetime in the ISM (e.g., Dwek et al. 2009).

Spitzer Space Telescope observations of SNRs have revealed ejecta dust in many SNRs with estimated masses in the $0.02\text{--}0.1 M_{\odot}$ range (Sugerman et al. 2006; Rho et al. 2008, 2009; Temim et al. 2010, 2012b), but the recent far-IR observations that are sensitive to cooler dust are now suggesting even larger masses. Cas A appears to contain $0.075 M_{\odot}$ of cool (~ 35 K) ejecta dust located on interior of the reverse shock (Barlow et al. 2010; Sibthorpe et al. 2010). Based on recent *Herschel*

observations, Matsuura et al. (2011) reported $0.4\text{--}0.7 M_{\odot}$ of cool dust in SN 1987A, while Gomez et al. (2012) find as much as $0.24 M_{\odot}$ of cool dust in the Crab Nebula.

While these recent results imply that SNe may indeed be major suppliers of dust, the masses in each each of these cases are derived using somewhat simplified models that consist of one or two dust temperature components. A more realistic scenario is to identify the heating source in the ejecta, and use a continuous size distribution of grains with each grain heated to a different temperature that depends on its composition, size and optical properties.

In this work, we present a detailed model of the physical mechanism giving rise to the observed IR emission from the Crab Nebula. Dust in the Crab Nebula was discovered as an IR excess above the synchrotron power-law spectrum of its pulsar wind nebula (PWN) (Trimble 1977; Glaccum et al. 1982; Marsden et al. 1984; Douvion et al. 2001; Green et al. 2004; Temim et al. 2006). Absorption features from dust are observed to spatially coincide with the ejecta filaments (Woltjer & Veron-Cetty 1987; Fesen & Blair 1990; Hester et al. 1990; Blair et al. 1997; Loll 2010), and a recent analysis of the *Spitzer* IRS spectra confirmed that the dust is indeed located in the filament cores (Temim et al. 2012b), and therefore dust that condensed in the ejecta.

The model considers three distinct dust compositions, each characterized by a power-law distribution in grain radii. The primary goal of our study is to determine whether a physical model for the IR emission, character-

¹ Observational Cosmology Lab, Code 665, NASA Goddard Space Flight Center, Greenbelt, MD 20771, USA

² Oak Ridge Associated Universities (ORAU), Oak Ridge, TN 37831, USA; tea.temim@nasa.gov

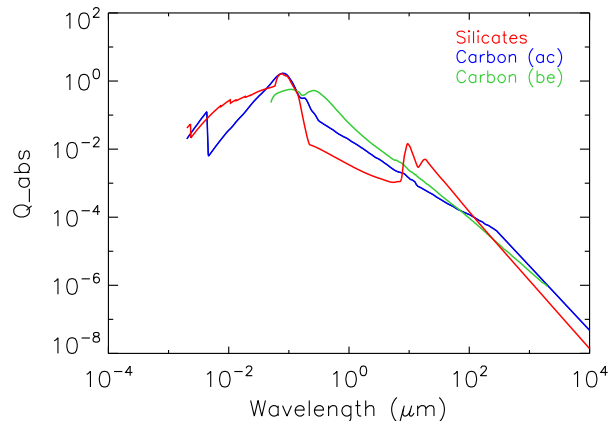


FIG. 1.— Absorption coefficients as a function of wavelength for silicate and amorphous carbon (BE) grains from Zubko et al. (2004) are shown in red and green, and amorphous carbon (AC) grains from Rouleau & Martin (1991) in blue.

ized by a continuous distribution in dust temperatures will affect the derived dust mass in this remnant. Our choice of the Crab Nebula is primarily motivated by the fact that the dust grains are heated by the synchrotron radiation from the PWN, so that their temperature can be accurately derived for each size and composition. Furthermore, since the newly-formed dust has neither been processed by the reverse shock, nor mixed with the ambient medium, the Crab Nebula offers a unique opportunity to study the mass, composition, and size distribution of pristine SN-condensed dust.

In spite of the fact that we concentrate on modeling the IR emission from the Crab Nebula, our results have global implications for deriving dust masses from IR observations, namely, that single or two (warm, cold) temperature representations of spectra can result in a significant overestimate of dust mass.

2. DUST HEATING MODEL

2.1. Heating by the PWN

Since the dust in the Crab Nebula is concentrated in the Rayleigh-Taylor filaments that form a cage around the PWN (Temim et al. 2012b), we model the heating of dust by assuming that the heating source is located at the center of the Crab Nebula, at the location of the Crab pulsar. In Temim et al. (2012b), we showed that the dominant heating source for the dust in the Crab Nebula is the synchrotron radiation from the PWN, with an insignificant possible contribution from collisional heating by the gas in the filaments. In this case, the heating rate of a single dust grain of radius a is given by

$$H(a) = \frac{\pi a^2 \int L_\nu(\nu) Q_{abs}(\nu, a) d\nu}{4\pi r^2}, \quad (1)$$

where L_ν is the non-thermal specific luminosity of the Crab Nebula's PWN, a is the grain size, $Q(\nu, a)$ is the absorption coefficient for a given grain composition, and r is the distance between the radiation source and the dust grain. The non-thermal luminosity $L_\nu(\nu)$ of the Crab Nebula's PWN that was used in our model is summarized in Figure 2 of Hester (2008). As described in Temim et al. (2012b), we consider $L_\nu(\nu)$ up to an en-

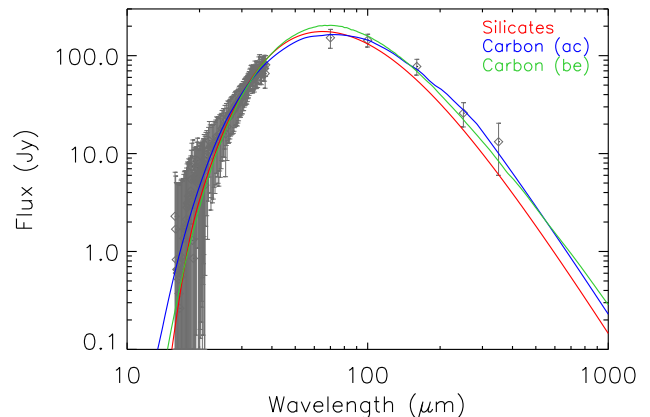


FIG. 2.— Best-fit dust grain heating models for three different grain compositions (see Figure 1). The data includes the average *Spitzer* IRS dust spectrum (Temim et al. 2012b), and the dust fluxes from *Herschel* PACS and SPIRE (Gomez et al. 2012). The best-fit parameters are summarized in Table 1, and corresponding total dust masses in Table 2.

ergy of about 0.6 keV, since we find that the fraction of the energy deposited in the dust at higher energies makes a negligible contribution of less than 1 %, due to the combined effects of decreasing of both $L_\nu(\nu)$ with energy, and the efficiency of the energy deposited by the photoelectrons in the dust grain (Dwek & Smith 1996).

Based on the three-dimensional models of the Crab Nebula, the ejecta filaments are located between 0.55-1.0 pc from the center of the nebula (e.g. Čadež et al. 2004). In our dust model, we allow the distance from the heating source r to vary between 0.5-1.5 pc in intervals of 0.2 pc. We allow the upper limit on the distance to extend beyond the physical location of the filaments in order to account for any attenuation by dust that would affect the heating rate. The best-fit models described in Section 3 favor the low end of the distance range, suggesting that the internal absorption in the nebula is negligible. In Temim et al. (2012b), we find that the optical depth is indeed low, with $\tau \leq 1$.

In equilibrium, the heating rate in Equation (1) of each grain of radius a is equal to the radiative cooling rate given by

$$L_{gr}(a) = 4\pi a^2 \int \pi B_\nu(\nu, T) Q(\nu, a) d\nu, \quad (2)$$

where B_ν is the Planck function and T is the dust grain temperature (Dwek & Werner 1981; Dwek et al. 2008). We used this relationship to compute the temperature for each grain radius and composition, and each distance r , and produced a final set of dust emission models by convolving the resulting emission spectrum for each grain size with the size distributions functions described in the previous section.

2.2. Dust Composition

The IR spectrum of dust in the Crab Nebula is fairly featureless (Temim et al. 2012b), consistent with the generally featureless spectra generated by silicate and carbon grains. Theoretical dust condensation models do indeed show that the largest fraction of dust formed in Type IIp SNe is in the form of silicate and carbon (e.g.

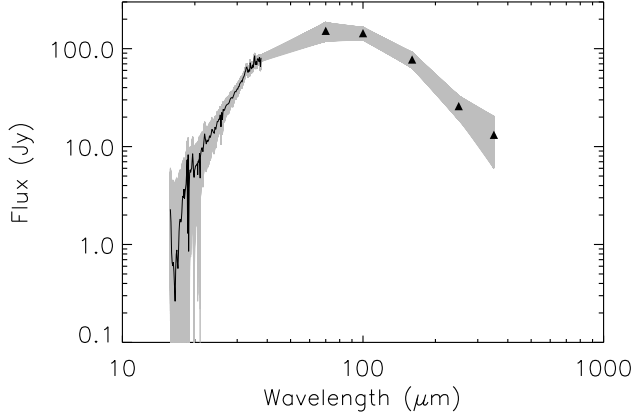


FIG. 3.— The range of spectra simulated by the Monte Carlo method described in Section 2.5 is shown as the gray band, with the actual data overlaid in black.

Kozasa et al. 2009).

We use three different sets of optical constants to calculate the absorptions coefficients $Q_{abs}(\nu, a)$: those from Weingartner & Draine (2001) to characterize the silicate grains; those from Rouleau & Martin (1991) to characterize the amorphous carbon grains (labeled AC throughout the paper); and those from Zubko et al. (2004) for amorphous carbon grains of type BE. The absorption coefficient as a function of wavelength for each of the three grain compositions is shown in Figure 1. We note that $Q_{abs}(\nu, a)$ for the BE carbon does not have coverage below $\sim 0.1 \mu\text{m}$, where a significant fraction of the energy absorption takes place. We only included them in this work for comparison with previous work by Temim et al. (2012b) and Gomez et al. (2012). We later show that the lack of short wavelength coverage for the optical constants significantly impacts the results of the dust heating model.

2.3. Grain Size Distributions

IR observations of unmixed young remnants, such as Cas A or SNR 1987A, have been used to derive the dust composition and mass, since determination of the grain size distribution requires detailed knowledge of the physical condition in the ejecta, and the dust heating mechanism. The size distribution of SN condensed dust is therefore a priori unknown. Models for the formation of dust in SNe (Todini & Ferrara 2001; Nozawa et al. 2010) have derived the size distribution of the various dust species that formed in the ejecta. However, these calculations assumed a uniform ejecta, and that the growth of the dust grains proceeded only through the accretion of single monomers, leaving out possible growth through coagulation in the ejecta.

Considering the above mentioned uncertainties, we adopt a general parametrization for the grain size distribution, described by a power law in grain radii, $a^{-\alpha}$, and a lower and upper grain radius cutoff on the grain radii, a_{min} and a_{max} respectively. Historically, such characterization was used by Mathis et al. (1977) (MRN) to derive the size distribution of interstellar dust from the observed UV-optical extinction (for a review see Clayton et al. 2003). The incorporation of additional observational constraints: the diffuse IR emission, in-

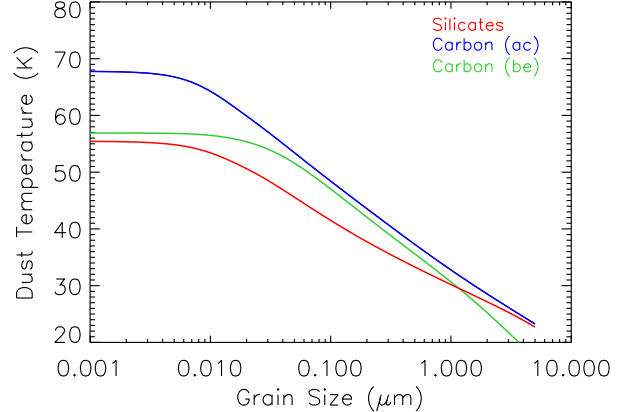


FIG. 4.— Grain temperature as a function of grain size for dust in the Crab Nebula. The input spectrum of the heating source is the broadband non-thermal spectrum of the Crab Nebula, as summarized in Figure 2 of Hester (2008). The dust grains are found to be located 0.5 pc from the center of the PWN. The colored curves correspond to grains with absorption coefficients shown in Figure 1.

terstellar abundances, and diffuse interstellar scattering, have yielded a more complex interstellar grain size distribution (Weingartner & Draine 2001; Li & Draine 2001; Zubko et al. 2004). This distribution is determined by the size distribution of the grains that are injected from all sources into the ISM, and by the various interstellar processes that alter their sizes, including thermokinetic sputtering, evaporative and shattering grain-grain collisions, accretion and coagulation. Attempts to characterize the net size distribution resulting from all these processes were made by (Liffman & Clayton 1989; O'Donnell & Mathis 1997; Hirashita 2012).

In order to fit the mid and far-IR dust emission in the Crab Nebula, we constructed a grid of grain size distributions with the power-law index α ranging from 0.0-4.0, and a_{max} ranging from 0.03 to $5.0 \mu\text{m}$. By allowing a_{max} to vary, we hope to determine to what size SN grains grow, and to compare the best-fit parameters to theoretical models for grain growth in Type IIP SNe. Fitting the minimum grain size cut-off a_{min} allows us to estimate the amount of future grain processes in SNRs. In the case of the Crab Nebula, we fixed a_{min} to $0.001 \mu\text{m}$ since the minimum grain size cut-off cannot be constrained by our mid-IR spectrum. In addition, since the dust in the Crab is radiatively heated by the PWN and the reverse shock has not yet reached the PWN, we do not expect that any grain destruction has yet occurred. Fixing a_{min} will not affect our final dust mass estimate since the mass of these smaller grains is negligible compared to the grains emitting in the far-IR (see Temim et al. 2012b; Gomez et al. 2012).

2.4. Fitting of the IR Spectrum

We fitted our entire grid of models to the observed dust emission from the Crab Nebula that include the average *Spitzer* IRS spectrum of the dust emission scaled to the total synchrotron and line-subtracted MIPS $24 \mu\text{m}$ flux (Temim et al. 2012b), the synchrotron and line-subtracted *Herschel* PACS 70, 100, and $160 \mu\text{m}$ flux measurements and the SPIRE 250 and $350 \mu\text{m}$ measurements

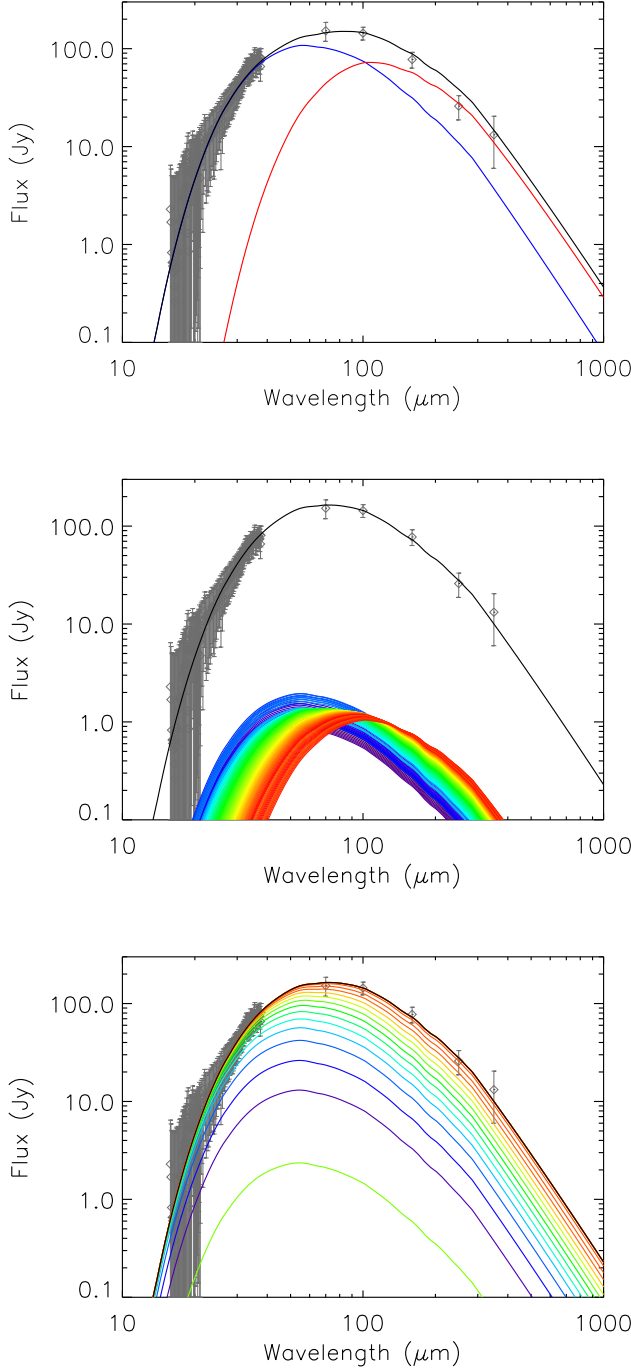


FIG. 5.— *Top*: Best-fit two-temperature carbon (BE) fit as used in Gomez et al. (2012). The blue curve represents the warm grains with a temperature of 63 K, while the red curve represents the cold 34 K grains. The black curve is the sum of the individual components. *Middle*: Our best-fit dust heating model for carbon (AC) grains. The rainbow colored curves represent individual spectra of dust grains of different sizes that are heated to a range of temperatures from 35–68 K. The black curve represents the sum of the individual rainbow-colored spectra. *Bottom*: The same model as in the middle plot, but with the individual spectra added cumulatively.

TABLE 1
BEST-FIT MODEL PARAMETERS

Composition	r (pc)	α	a_{max} (μm)	χ^2
Silicates	0.5	3.5 ± 0.1	$5.0^{+...}_{-0.5}$	27.1
Carbon (AC)	0.5	3.5 ± 0.1	0.6 ± 0.2	11.7
Carbon (BE)	0.5	3.5 ± 0.1	> 1.0	30.7

NOTE. — Best-fit model parameters where r is the distance of the dust grains from the center of the PWN, α is the power-law index on the grain size distribution, and a_{max} is the maximum grain size cut-off. The uncertainties on the parameters for each grain composition were found from Monte Carlo simulations described in Section 2.5.

(Gomez et al. 2012), where cold dust emission still contributes. The data and the best-fit model for each grain composition are shown in Figure 2. The best-fit distance r for all compositions is 0.5 pc, while the best-fit values for the power-law size distribution index α and the maximum grain size cut-off a_{max} are summarized in Table 1. The dust model for the amorphous carbon (AC) grain composition provides the best fit to the data, since it simultaneously provides a good fit to the mid-IR spectrum and the *Herschel* data points at far-IR wavelengths. The best-fit silicate grain composition falls somewhat short at far-IR wavelengths, while the carbon (BE) composition slightly underestimates the IRS spectrum in the mid-IR.

2.5. Monte Carlo Simulations

We note that the large uncertainties in the data points in the IRS spectrum are dominated by systematic uncertainties introduced by the subtraction of the underlying synchrotron spectrum (see Temim et al. 2012b). For this reason, the reduced χ^2 for our best fits is too small, on the order of ~ 0.06 . Since our uncertainties are not random statistical uncertainties, we cannot use χ^2 statistics in determining confidence levels for our fitted parameters. Instead, we used a Monte Carlo simulation to estimate the spread in our fitted parameters. The absolute χ^2 values from our fits are used only to demonstrate the relative goodness of fit for the various models.

In order to estimate the uncertainties in the fitted parameters while correctly accounting for the statistical uncertainties in the dust spectrum introduced by the subtraction of the synchrotron spectrum, we generated 5,000 simulated spectra using the Monte Carlo method. The spectra were simulated by adding an average global synchrotron spectrum to the IRS data, with a synchrotron power-law index of 0.42, as found by Gomez et al. (2012). We then produced 5,000 sample dust spectra by re-subtracting a global synchrotron spectrum while randomly selecting spectral indices within 3σ (± 0.02) of the best fit value of 0.42. We also randomly selected values for the $3.6 \mu\text{m}$ flux from which the synchrotron spectrum is extrapolated in the range of 12.65 ± 0.63 Jy (Temim et al. 2012b), and we accounted from the $\sim 5\%$ uncertainty that results from normalizing the IRS dust spectrum to the total flux from dust in the MIPS $24 \mu\text{m}$ band. The *Spitzer* MIPS and *Herschel* data were similarly varied within the uncertainties listed in Table 4 of Gomez et al. (2012). The resulting range of simulated spectra are shown as the gray band in Figure 3, with the actual data overlaid in black. We then fitted our grid of

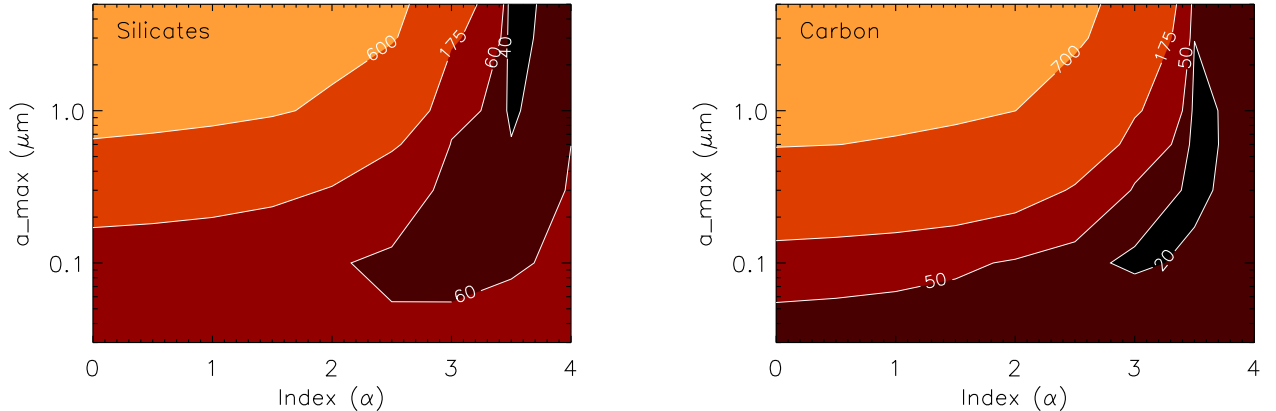


FIG. 6.— χ^2 contour plots for the maximum grain size cutoff a_{\max} and the index on the power-law grain size distribution α . The contours indicate that an α of 3.5 and a larger grain size cutoff ($> 0.1 \mu\text{m}$) tend to produce better fits for both silicate and carbon (AC) grain compositions.

dust distribution models to each of the simulated spectra to obtain a distribution in the best-fit values for the dust distribution power-law index α , a_{\max} , and the total dust mass for each composition. The results for each parameter will be discussed in the following sections.

3. RESULTS AND DISCUSSION

3.1. Distribution of Grain Temperatures

The main difference in using a physical dust heating model that allows for a distribution of grain sizes, rather than using two-component fits for two distinct temperatures, is the resulting continuous distribution of dust grain temperatures that will determine the shape of the total dust emission spectrum. Figure 4 shows the dust temperature (T) as a function of grain size, assuming that the heating source (i.e. the Crab’s PWN) is located at the best-fit distance of 0.5 pc. The colored curves show the temperature profiles for each of the three grain compositions that were used in the fit. The shape of the temperature profile depends on the product $L_\nu Q_{abs}(\nu, a)$, integrated of the available frequency range. An important thing to notice is the significant difference in temperature of the smaller grains between the carbon (AC) and carbon (BE) compositions. While the carbon (AC) grains with sizes below $\sim 0.01 \mu\text{m}$ are heated to a temperature of ~ 68 K, the same-sized carbon (BE) grains are only heated to ~ 55 K. The large difference in dust temperatures between these two carbon compositions is not due to the differences in grain properties or the shape of the absorption coefficients Q_{abs} , but is instead primarily due to the available wavelength coverage of Q_{abs} . In Section 2.1, we mentioned that we only consider L_ν up to an energy of about 0.6 keV since the energy deposited in the dust above this energy becomes negligible. However, the absorption coefficients for the carbon (BE) grains are only available down to a wavelength $0.05 \mu\text{m}$, which means that L_ν was only integrated up to an energy of 0.02 keV. Accounting for energies above 0.02 keV is especially important for heating by PWNe, since their non-thermal spectra peak at these energies. The carbon (AC) composition therefore provides a more physical dust heating model for the Crab. The additional coverage between 0.002 and $0.05 \mu\text{m}$ (0.02–0.6 keV) for

the carbon (AC) grains raises the temperature for all grain sizes, but has a most apparent affect on the smaller grains (see Figure 4). This significant difference in dust temperature emphasizes the importance of using grain compositions with adequate wavelength coverage for the absorption coefficient when constructing models to describe dust emission in SNRs, especially dust surrounding PWNe.

Figure 5 shows the comparison between a two-temperature fit to the dust emission in the Crab Nebula using a carbon (BE) composition (top panel), as in Gomez et al. (2012), and our best-fit model for the carbon (AC) grains with parameters listed in Table 1 (middle and bottom panels). The middle panel of Figure 5 shows spectra of grains with different sizes as individual rainbow colored curves that all add up to the best-fit black curve. The bottom panel shows the same model, but with every tenth cumulative sum of individual spectra shown in rainbow colors. While both models provide equally good fits to the IR data, the physical dust heating model allows us to constrain physical properties of the dust, and significantly affects the total dust mass responsible for the IR emission (see Section 3.3).

3.2. Grain Size Distribution

The dust heating model also allows us to place some constraints on the shape of the grain size distribution and the maximum size of grains that formed in the Crab Nebula. Figure 6 shows the χ^2 contour plots for α , the index of the power-law size distribution, versus the maximum grain size cut-off a_{\max} . The parameter values for models with minimum χ^2 values are listed in Table 1. The contour plots show the relative goodness of fit for the range of parameter values used in our grid of dust distribution models. For all compositions, the best-fit value for the power-law index is $\alpha=3.5$. The fits to the 5,000 Monte Carlo simulations show that the power-law index is very well constrained with a standard deviation of only 0.1. This is the same size distribution that is found for the ISM (e.g. Mathis et al. 1977). Physical modeling of dust emission for a larger sample of SNRs is needed to determine if similar size distributions are found in other core-collapse SNe.

In Temim et al. (2012b), we found that the dust emis-

TABLE 2
TOTAL DUST MASS (M_{\odot})

Composition	Observations		Nucleosynthesis Models		
	This Work	Gomez et al. (2012)	WW95	N07	WH07
Silicates	0.128 ± 0.004	$0.24^{+0.32}_{-0.08}$	0.08	0.32	0.12
Carbon (AC)	0.027 ± 0.003	...	0.05	0.10	0.11
Carbon (BE)	0.050 ± 0.002	0.11 ± 0.01	0.05	0.10	0.11

NOTE. — . The uncertainties on the dust mass from this work were found from Monte Carlo simulations described in Section 2.5. The dust mass listed for the nucleosynthesis models is the maximum allowed dust mass assuming a 100% condensation efficiency, and the yields for a $11 M_{\odot}$ progenitor from Woosley & Weaver (1995) (WW95), and a $13 M_{\odot}$ progenitor from Nomoto et al. (2006) (N07) and Woosley & Heger (2007) (WH07).

sion in the Crab observed by *Spitzer* implies a small grain size of $< 0.05 \mu\text{m}$. However, since we only had coverage up to $70 \mu\text{m}$, we were sampling only the smaller grains that were heated to temperatures of around 50 K (see Figure 4). The addition of the *Herschel* long wavelength data has now allowed us to place constraints on the maximum size of dust grains in the Crab’s filaments. Our best-fit model appears to favor a fairly large maximum grain size cut-off (see Figure 6). The value for a_{max} for the best-fit model is $0.6 \mu\text{m}$ or larger, depending on the grain composition (Table 1). This is actually more consistent with models of dust formation in Type IIP SNe (Kozasa et al. 2009; Nozawa et al. 2010). These models show that the dust mass of grains formed in Type IIP SNe with massive H-envelopes is dominated by grains larger than $0.03 \mu\text{m}$, while the mass of dust for Type IIb SNe is dominated by very small grain $< 0.006 \mu\text{m}$. Probing the dust grain size in SNRs can therefore be an extremely useful tool for investigating the properties of the SN progenitor. The Crab Nebula is thought to be a result of a Type IIP explosion, primarily based on the low expansion velocities of the ejecta filaments and the low progenitor mass (e.g. Chevalier 2005; MacAlpine & Satterfield 2008). The large dust grain radii inferred from our models are consistent with a Type IIP origin. We note that the larger grain size also implies that a large fraction of the dust mass will survive the eventual reverse shock interaction (Dwek 2005; Kozasa et al. 2009; Bianchi et al. 2009; Nozawa et al. 2010).

3.3. Revised Dust Mass for the Crab Nebula

The total dust mass for the Crab Nebula that results from our heating model is $0.128 \pm 0.004 M_{\odot}$ and $0.027 \pm 0.003 M_{\odot}$ for silicate and carbon (AC) grains, respectively (Table 1). Figure 7 shows the histograms of the total dust mass for the best-fit model for each of the 5,000 simulated spectra. A Gaussian distribution was fitted to the histogram and its mean and σ taken as the estimated mass and its uncertainty. The plots show that the total mass is very well constrained for both silicate and carbon grain compositions. We note that the total mass for each composition is significant lower than the masses estimated from the two-component temperature fits; $0.24^{+0.32}_{-0.08} M_{\odot}$ for silicates and $0.11 \pm 0.01 M_{\odot}$ for carbon (Gomez et al. 2012) (see Table 2). The silicate and carbon (BE) compositions that we used in our fits are the same as those used in (Gomez et al. 2012), and we confirmed this by reproducing their total dust masses

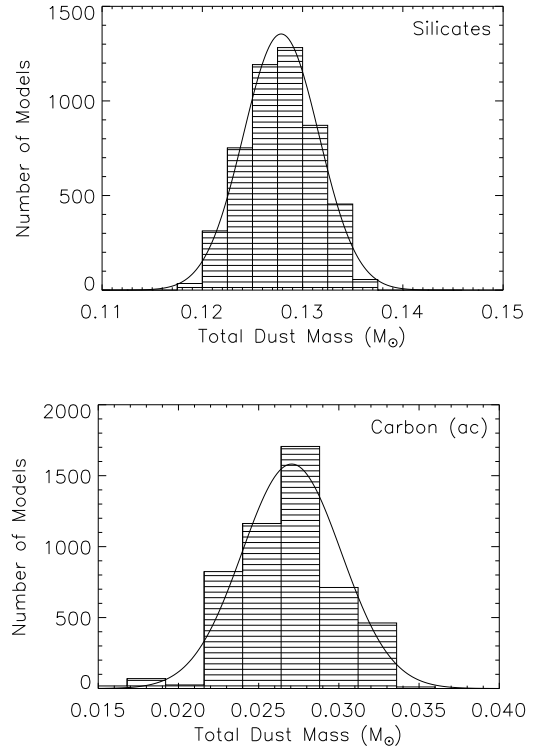


FIG. 7.— Distribution of total dust masses from the fits to 5000 Monte Carlo simulations of the IR data using silicate (top) and carbon (AC) grains (bottom). The best-fit Gaussian is overplotted on the histograms as a solid black line. We use the mean and standard deviation of the Gaussian for the best-fit total mass and uncertainty, $0.128 \pm 0.004 M_{\odot}$ for silicates and $0.027 \pm 0.003 M_{\odot}$ for carbon grains.

with a two-temperature dust fit. We find that if we use these same absorption coefficients in our dust heating model, the total mass of dust is reduced by a factor of ~ 2 . The total mass for carbon grains is lowered even further by using more realistic Q_{abs} values with coverage at lower wavelengths. As discussed in Section 3.1, using the carbon (AC) grains raises the temperature of the smaller grains, which will in turn contribute more flux to the spectrum and lower the required number of large cooler grains that dominate the mass. The significantly different mass estimates are therefore the results of a combination of a physical grain size and temperature distribution, and a selection of well measured absorption coefficients that will account for the absorption of higher

energy photons.

The fact that carbon (AC) grains provide a significantly better fit to the dust emission in the Crab Nebula suggests that the dust mass may either be dominated by carbon grains, or possibly a mixture of carbon and silicate grains. The total mass estimated from silicates should therefore be treated as an upper limit, and the lower carbon mass of $0.027 \pm 0.003 M_{\odot}$ as a more realistic estimate for the total dust mass in the Crab Nebula. This lower dust mass is further supported by nucleosynthetic yields from core-collapse SNe for progenitors in the 11-13 M_{\odot} range (Woosley & Weaver 1995; Woosley & Heger 2007; Nomoto et al. 2006). We assumed a 100% grain condensation efficiency and calculated the upper limit on the carbon and silicate grain mass from the total yield of carbon, oxygen, magnesium, silicon, and iron. To obtain the upper limit on the silicate grain mass, we summed the maximum possible masses for SiO_2 , MgO , and Fe_3O_4 grains. The results are listed in Table 2, and they show that the Gomez et al. (2012) mass estimates are clearly too large, especially considering that the progenitor of the Crab Nebula is estimated to be around $\sim 9.5 M_{\odot}$ (MacAlpine & Satterfield 2008). The total mass of silicate dust derived from our models is also too large compared to nucleosynthesis yields, suggesting that the dust in the Crab Nebula is mostly in the form of carbon grains. This work implies that a physical dust model that allows for continuous size and temperature distributions will revise the total dust mass estimates for many SNRs, especially the recent estimates made from fitting simplified two-component models to account for the far-IR emission, including the controversially high mass of $0.4 - 0.7 M_{\odot}$ found for SN 1987 A (Matsuura et al. 2011).

4. CONCLUSIONS

We modeled the mid and far-IR dust emission from the Crab Nebula in order to constrain the dust grain properties and total dust mass. We use a physical dust heating model in which a continuous power-law size distribution of dust grains is radiatively heated by the PWN.

The best-fit models favors a grain size distribution with a power-law index of 3.5, and a relatively large maximum grain size cut-off of $> 0.6 \mu\text{m}$, consistent with theoretical predictions of dust formation in Type IIP SNe (Kozasa et al. 2009; Nozawa et al. 2010). The IR emission is best described by an amorphous carbon grain composition with a total mass of $0.027 \pm 0.003 M_{\odot}$, significantly lower than previous estimates from more simplified two-temperature models. The difference in the dust mass is due to a combination of fitting a continuous grain size and temperature distribution, and applying grain absorption coefficients with a more complete wavelength coverage that allows us to account for heating from higher energy photons from the PWN.

In recent years, most large dust mass estimates for SNRs assumed the simplified one or two-temperature models, including the mass estimates from *Herschel* data for Cas A, SN 1987 A, and the Crab Nebula (e.g. Barlow et al. 2010; Sibthorpe et al. 2010; Matsuura et al. 2011; Gomez et al. 2012). Our modeling results imply that a more realistic dust emission model will revise, and may significantly reduce the mass estimates for many SNRs. The amount of SN-condensed dust in the Crab Nebula is significantly lower than that required to produce the massive amount of dust observed in high-redshift galaxies even if the dust is not destroyed in the ISM (Dwek et al. 2007).

This will have important implications on the questions of dust production in SNe and its ultimate survival. While the model presented in this paper assumes radiatively heated dust, we are also combining varying grain size distributions with a dust heating model for collisionally heated grains (see Arendt et al. 2010; Temim et al. 2012a). We plan to apply our models to revise dust mass estimates for a large number of PWNe and SNRs, and use them to constrain dust grain properties that may shed light on the nature of the SN progenitors.

We thank Rick Arendt and George Sonneborn for useful discussions and comments on the paper.

REFERENCES

- Arendt, R. G., Dwek, E., Blair, W. P., et al. 2010, *ApJ*, 725, 585
 Barlow, M. J., Krause, O., Swinyard, B. M., et al. 2010, *A&A*, 518, L138
 Bianchi, S., Schneider, R., & Valiante, R. 2009, in *Astronomical Society of the Pacific Conference Series*, Vol. 414, *Cosmic Dust - Near and Far*, ed. T. Henning, E. Grün, & J. Steinacker, 65
 Blair, W. P., Davidson, K., Fesen, R. A., et al. 1997, *ApJS*, 109, 473
 Cherchneff, I., & Dwek, E. 2010, *ApJ*, 713, 1
 Chevalier, R. A. 2005, *ApJ*, 619, 839
 Clayton, G. C., Wolff, M. J., Sofia, U. J., Gordon, K. D., & Misselt, K. A. 2003, *ApJ*, 588, 871
 Douvion, T., Lagage, P. O., Cesarsky, C. J., & Dwek, E. 2001, *A&A*, 373, 281
 Dwek, E. 2005, in *American Institute of Physics Conference Series*, Vol. 761, *The Spectral Energy Distributions of Gas-Rich Galaxies: Confronting Models with Data*, ed. C. C. Popescu & R. J. Tuffs, 103-122
 Dwek, E., Galliano, F., & Jones, A. 2009, in *Astronomical Society of the Pacific Conference Series*, Vol. 414, *Cosmic Dust - Near and Far*, ed. T. Henning, E. Grün, & J. Steinacker, 183
 Dwek, E., Galliano, F., & Jones, A. P. 2007, *ApJ*, 662, 927
 Dwek, E., & Smith, R. K. 1996, *ApJ*, 459, 686
 Dwek, E., & Werner, M. W. 1981, *ApJ*, 248, 138
 Dwek, E., Arendt, R. G., Bouchet, P., et al. 2008, *ApJ*, 676, 1029
 Fesen, R., & Blair, W. P. 1990, *ApJ*, 351, L45
 Glaccum, W., Harper, D. A., Loewenstein, R. F., Pernic, R., & Low, F. J. 1982, in *Bulletin of the American Astronomical Society*, Vol. 14, *Bulletin of the American Astronomical Society*, 612
 Gomez, H. L., Krause, O., Barlow, M. J., et al. 2012, *ApJ*, 760, 96
 Green, D. A., Tuffs, R. J., & Popescu, C. C. 2004, *MNRAS*, 355, 1315
 Hester, J. J. 2008, *ARA&A*, 46, 127
 Hester, J. J., Graham, J. R., Beichman, C. A., & Gautier, III, T. N. 1990, *ApJ*, 357, 539
 Hirashita, H. 2012, *MNRAS*, 422, 1263
 Kozasa, T., Nozawa, T., Tominaga, N., et al. 2009, in *Astronomical Society of the Pacific Conference Series*, Vol. 414, *Cosmic Dust - Near and Far*, ed. T. Henning, E. Grün, & J. Steinacker, 43
 Li, A., & Draine, B. T. 2001, *ApJ*, 554, 778
 Liffman, K., & Clayton, D. D. 1989, *ApJ*, 340, 853
 Loll, A. 2010, PhD thesis, Arizona State University
 MacAlpine, G. M., & Satterfield, T. J. 2008, *AJ*, 136, 2152
 Marsden, P. L., Gillett, F. C., Jennings, R. E., et al. 1984, *ApJ*, 278, L29
 Mathis, J. S., Ruml, W., & Nordsieck, K. H. 1977, *ApJ*, 217, 425
 Matsuura, M., Dwek, E., Meixner, M., et al. 2011, *Science*, 333, 1258

- Nomoto, K., Tominaga, N., Umeda, H., Kobayashi, C., & Maeda, K. 2006, *Nuclear Physics A*, 777, 424
- Nozawa, T., Kozasa, T., Tominaga, N., et al. 2010, *ApJ*, 713, 356
- O'Donnell, J. E., & Mathis, J. S. 1997, *ApJ*, 479, 806
- Rho, J., Kozasa, T., Reach, W. T., et al. 2008, *ApJ*, 673, 271
- Rho, J., Reach, W. T., Tappe, A., et al. 2009, in *Astronomical Society of the Pacific Conference Series*, Vol. 414, *Cosmic Dust - Near and Far*, ed. T. Henning, E. Grün, & J. Steinacker, 22
- Rouleau, F., & Martin, P. G. 1991, *ApJ*, 377, 526
- Sibthorpe, B., Ade, P. A. R., Bock, J. J., et al. 2010, *ApJ*, 719, 1553
- Silvia, D. W., Smith, B. D., & Shull, J. M. 2012, *ApJ*, 748, 12
- Sugerman, B. E. K., Ercolano, B., Barlow, M. J., et al. 2006, *Science*, 313, 196
- Temim, T., Slane, P., Arendt, R. G., & Dwek, E. 2012a, *ApJ*, 745, 46
- Temim, T., Slane, P., Reynolds, S. P., Raymond, J. C., & Borkowski, K. J. 2010, *ApJ*, 710, 309
- Temim, T., Sonneborn, G., Dwek, E., et al. 2012b, *ApJ*, 753, 72
- Temim, T., Gehr, R. D., Woodward, C. E., et al. 2006, *AJ*, 132, 1610
- Todini, P., & Ferrara, A. 2001, *MNRAS*, 325, 726
- Trimble, V. 1977, *Astrophys. Lett.*, 18, 145
- Čadež, A., Carramiñana, A., & Vidrih, S. 2004, *ApJ*, 609, 797
- Weingartner, J. C., & Draine, B. T. 2001, *ApJS*, 134, 263
- Woltjer, L., & Veron-Cetty, M.-P. 1987, *A&A*, 172, L7
- Woosley, S. E., & Heger, A. 2007, *Phys. Rep.*, 442, 269
- Woosley, S. E., & Weaver, T. A. 1995, *ApJS*, 101, 181
- Zubko, V., Dwek, E., & Arendt, R. G. 2004, *ApJS*, 152, 211